

Directed force chain networks and stress response in static granular materials

J. E. S. Socolar¹, D. G. Schaeffer², and P. Claudin³

¹ Department of Physics and Center for Nonlinear and Complex Systems, Duke University, Durham, NC 27708, USA

² Department of Mathematics and Center for Nonlinear and Complex Systems, Duke University, Durham, NC 27708, USA

³ Laboratoire des Milieux Désordonnés et Hétérogènes (UMR 7603), 4 place Jussieu - case 86, 75252 Paris Cedex 05, France

June 29, 2019

Abstract. A theory of stress fields in two-dimensional granular materials based on directed force chain networks is presented. A general Boltzmann equation for the densities of force chains in different directions is proposed and a complete solution is obtained for a special case in which chains lie along a discrete set of directions. The analysis and results demonstrate the necessity of including nonlinear terms in the Boltzmann equation. A line of nontrivial fixed point solutions is shown to govern the properties of large systems. In the vicinity of a generic fixed point, the response to a localized load shows a crossover from a single, centered peak at intermediate depths to two propagating peaks at large depths that broaden diffusively.

PACS. 45.70.Cc Static sandpiles; granular compaction – 83.80.Fg Granular solids

1 Introduction

The response to a localized force applied at the boundary of a semi-infinite sample is an essential feature of any macroscopic material. For materials that are well described by linear elasticity theory, the response can be calculated by standard techniques: using the relation of the stresses to a displacement field, one constructs partial differential equations for components of the stress tensor σ , then solves them with appropriate boundary conditions on σ and its derivatives. For a wide class of granular materials, however, the absence of an energy expressible in terms of microscopic (or grain scale) displacements leads to serious difficulties in deriving the stress response.

Numerous attempts have been made, many quite recent, to close the system of stress equilibrium equations by deriving (or simply guessing) a relation between the components of the stress tensor beyond those required by Newton's laws. The needed relation may be extracted from assumptions concerning yield thresholds in elasto-plastic theories [1,2], from an analysis of physics at the grain scale,[3], from general symmetry principles and considerations of simplicity [4,5], or from considerations applicable to isostatic networks [6,7]. A special case that has received much attention is that of frictionless, circular disks.[8,9] Alternatively, lattice models for the configuration of individual inter-grain forces can serve as the basis for the derivation of average stress patterns while simultaneously addressing the statistical properties of forces at the grain scale. [4,10,11,12]

In this paper we develop a theory of stress distribution in noncohesive granular materials based on the physics of *force chains*, rather than macroscopic stresses or grain scale interactions. Experimental probes and numerical computations of stress patterns in granular materials universally show filamentary networks that support strong forces between grains. [13,14,15] We take this as motivation to describe all of the forces in the system in terms of linear “force chains” that combine to form a network whose large scale properties determine the macroscopic stress field. To describe such networks, Bouchaud et al. recently introduced the “ ΛY -model” (pronounced “double Y model”).[16] Here we develop the ΛY -model in greater detail, point out certain essential ways in which the original formulation and analysis was incomplete, and calculate stress patterns and response functions in special cases.

In the ΛY -model, stresses are modeled as networks of interacting line segments that carry compressive forces. A crucial feature of the model is that the force chains are *directed*: each is conceived as “propagating” from one of its endpoints to the other, in a sense that will be clarified below. Chains are created by three processes: (1) imposed conditions at a boundary; (2) the splitting of one chain into D in a manner that preserves force balance at the splitting point, where D is the spatial dimension of the material; or (3) the fusion of D chains into one. They then propagate until they are destroyed via splitting (“ Λ ” processes), fusion (“ Y ” processes), or traversal of a sample boundary. We refer to a static network of chains in

teracting in this way as a “directed force chain network” (DFCN).

Our goal is to determine the large scale structure of DFCN’s and their average responses to small, local perturbations at a boundary. We first develop a Boltzmann equation governing the spatial variations in the densities of chains supporting certain force intensities and oriented in particular directions.¹ We then seek solutions in the special case where the chains are restricted to lie along a discrete set of directions. The results highlight several subtle features of the directed force chain system, and show that the response of such systems can have a rich structure that includes some surprising effects.

Our primary result can best be stated with reference to the results previously obtained via standard elasticity theory or posited closure relations. In standard elasticity theories of two-dimensional isotropic systems, the response to a normal force applied at one point ($x = 0$) of a half plane is [17]

$$\sigma_{zz} = \frac{2}{\pi} \frac{z^3}{(x^2 + z^2)^2}, \quad (1)$$

where $z = 0$ at the surface and increases with depth. Thus at any fixed depth z , the response σ_{zz} consists of a single peak centered on $x = 0$, with a width that grows linearly with depth. Though σ_{zz} for anisotropic materials can have two peaks, the response in this geometry is always invariant under uniform dilations and rescaling: ($x \rightarrow ax$, $z \rightarrow az$) yields $\sigma_{ij} \rightarrow (1/a)\sigma_{ij}$.

In another class of theories based on closure relations that make no reference to a displacement field, the stress equilibrium equations are hyperbolic. In such cases, the response function consists of two peaks that propagate linearly away from $x = 0$. The inclusion of weak disorder in these models leads to a diffusive broadening of the peaks with increasing depth.[5] Note that this form of response differs markedly from the elastic case, as the ratio of peak width to propagation distance decreases like $1/\sqrt{z}$ at large depths rather than remaining constant. Perhaps even more importantly, the two types of theory require different manners of specifying boundary conditions. Whereas standard elasticity theory requires the specification of two conditions on the stresses (and/or their derivatives) at all points on the boundary, the hyperbolic models require (permit) the specification of stresses on only the top boundary.

In the directed force chains system, we find that both top and bottom boundary conditions are important, but the solutions and response functions in deep systems have a richer structure than either the elastic or hyperbolic theories suggest. For very shallow depths beneath the surface, the response may have one or two peaks, depending on the details of the applied forces. For intermediate depths, up to several times the average length of a force chain, the response has a single peak and may appear quite similar to a standard elastic response. For large depths, however,

two peaks emerge that grow diffusively with depth. This latter behavior suggests that at the largest scales a hyperbolic model for stress equilibrium may be appropriate even for systems with strong disorder, though important questions remain concerning the role of the discrete set of directions in sustaining the two-peaked structure.

A second result to be emphasized is the failure of the linearized theory obtained by assuming that all chain densities are small. Formally, this assumption is equivalent to neglecting the fusion of chains, keeping only those terms in the Boltzmann equation that describe splitting events. For intermediate and deep systems, internal consistency of the theory requires that the response be computed by linearizing around a nontrivial fixed point of the Boltzmann equation. This sheds new light on previous efforts to derive a linear elasticity theory of DFCN’s. It also has important implications for the numerical modeling of DFCN’s and the interpretation of experimental measurements of stress response in granular systems.

In addition to these two central results, we point out several curious features of DFCN’s in a simple slab geometry in two dimensions. These include an effective Poisson ratio that may depend on the way in which a load is applied, an exponentially localized region of increased horizontal stresses in the middle of a slab subject to horizontally uniform vertical stresses at top and bottom, and a distinction between responses to identical applied macroscopic stresses with different distributions of force chain densities in various directions.

The paper is organized as follows. In the Section 2, we introduce the concept of the directed force chain, define the constants, variables and functions that enter our theory, develop a Boltzmann equation that governs spatial variations of the densities of force chains, and discuss the boundary conditions on the equation. We then define a special case of the model in which chain directions are restricted to discrete set that is amenable to analytical treatment. In Section 3, we solve the discrete Boltzmann equation in a slab of depth z for the case of applied loads that are uniform in the horizontal direction, identifying the (nontrivial) solutions relevant for the computation of response functions. In Section 4, we analyze the response (in the discrete model) in the vicinity of a generic fixed point, present some results for other choices of discrete directions in 2D and describe a possible generalization to 3D. We also discuss the relation of our analysis methods to the long-wavelength theory presented in Ref. [16]. We conclude, in Section 6 with discussions of the issue of numerical generation of DFCN’s and some open questions.

2 Boltzmann equation for directed force chains

2.1 Definitions, the Boltzmann equation, and its boundary conditions

A *force chain* is defined as a line segment that supports a compressive force. The *direction* of a force chain has

¹ We use the term “Boltzmann equation” loosely. It does not imply the existence of a causal structure or H-theorem.

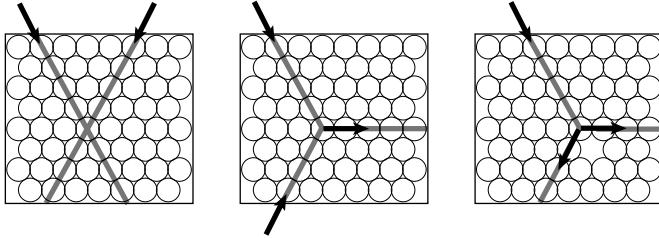


Fig. 1. Illustration of force chains. (a) Two force chains initiated at the top surface cross without interacting. (b) When one of the force chains is initiated at the bottom, a fusion becomes possible. (c) A force chain initiated at the top that splits upon encountering a defect.

two features. First, the segment makes a particular angle with the vertical. Second, the two ends of the segment are distinguished – the segment has a “beginning” and an “end” determined by the role the chain plays in the network. Fig. 1 illustrates the latter point. The figure shows a two-dimensional system consisting of a hexagonal array of grains. In panel (a), two forces are applied at the top boundary and the forces propagate along chains, crossing at the central grain. In panel (b), a similar situation is shown, but this time one of the chains is assumed to be specified by fixing its position at the bottom boundary instead of the top. In this case, a fusion of the two chains at the central grain is permitted (though not required) and the resulting configuration may be different, demonstrating the inequivalence of the two possible choices of direction for the chain whose boundary condition was changed. The horizontal chain is assumed to “begin” at the fusion point and “end” at the boundary.

Thus each chain has an intensity, f , and a direction $\hat{\mathbf{n}}$. Though we will sometimes combine the two and express them as a vector \mathbf{f} , it is important to keep in mind that the compressive force supported by the chain has no forward or backward direction. A grain that is part of a force chain experiences no net force, only a stress with its major principal axis along the chain. The distinction between the forward and backward directions of the chain refers to its own boundary conditions, which are ultimately related to the boundary conditions at the edge of the sample, though this relation may be difficult to determine.

In addition to fusion of chains, it is possible for a chain to split into two (in two dimensions). Fig. 1(c) shows a splitting event induced by the presence of a defect in the system. In general, ordered regions and defects will not be so easy to identify by eye, and all sites are assumed to produce splittings and permit fusions with probabilities drawn from a specified angular distribution, as described below.

To clarify the way in which directions may be assigned to force chains, it may be helpful to consider the configuration shown in Fig. 2. Here the question arises as to how one can assign a direction to the chain in the middle of panel (a). If the situation is as shown in (b), with boundary imposed at the two sites on the top surface, then the middle chain must be interpreted as consisting of two

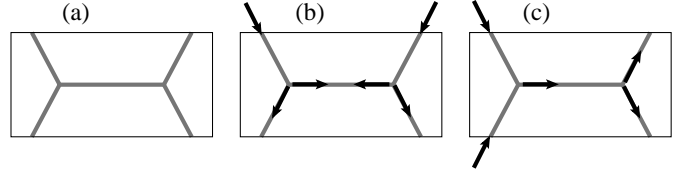


Fig. 2. (a) A seemingly ambiguous configuration of force chains. (b) Boundary conditions that imply an annihilation event. (c) Boundary conditions that give a unique direction to the middle chain.

oppositely directed chains that annihilate in the middle. The same is true for any other configuration of boundary conditions that force this configuration on the middle chain. Alternatively, there exist other possible specifications of the boundary conditions that give the middle chain a specific orientation, as shown in (c). In developing the theories below, we neglect all annihilations of the type shown in (b). The reason is that for very narrow force chains, the probability of two chains meeting head on is very low. In granular systems, it may be argued that the force chain widths are effectively of the order of a grain size, so that annihilation events are not entirely negligible. For the present paper, we neglect effects associated with the finite sizes of grains. Preliminary investigations strongly suggest that inclusion of terms corresponding to annihilations does not change the general features of the results.

For clarity of presentation, from here on we work in two dimensions unless explicitly noted otherwise. The main difference in D dimensions is that vertices where chains fuse or split generically require $D + 1$ chains in order to achieve force balance, since force balance among fewer chains would require the highly improbable event that one of them lie in the subspace spanned by the others.

We begin with the assumption that a 2D granular material can be thought of as a collection of local environments through which single force chains are either transmitted or split into two, and pairs of intersecting force chains either pass through each other or fuse into one. We also assume that the force chains carry all of the stresses in the system. Newton’s laws are built into the model via the constraint that the forces at each splitting and fusion event must balance. In this formulation of the model, there are never any unbalanced torques, as the three chains associated with a splitting or fusion always meet at a single point.

Following the suggestion of Ref. [16], we construct a Boltzmann equation governing the densities of chains as follows. Let $P(f, \hat{\mathbf{n}}, \mathbf{r})$ represent the probability of finding a force chain of intensity f in direction of unit vector $\hat{\mathbf{n}}$ passing through the spatial point \mathbf{r} . In other words, $\int_g^{g+\delta} df \int d\hat{\mathbf{n}} |\hat{\mathbf{n}} \cdot \hat{\mathbf{u}}| P(f, \hat{\mathbf{n}}, \mathbf{r})$ is the number of chains of intensity between g and $g + \delta$ that cross a unit length line segment through \mathbf{r} and perpendicular to $\hat{\mathbf{u}}$. Note that P has dimensions of $1/(force \times length)$ in 2D and cannot be negative. The local stress tensor, expressed in terms of

the coarse grained quantity P , is given by [16]

$$\sigma_{\alpha\beta} = \int_0^\infty df \int d\Omega n_\alpha n_\beta f P(f, \hat{\mathbf{n}}, \mathbf{r}). \quad (2)$$

Here Ω represents the D -dimensional angular direction of $\hat{\mathbf{n}}$ divided by the full solid angle so that $\int d\Omega = 1$. For our 2D discussion, we will use $\theta \in (-\pi, \pi]$ to designate the direction $\hat{\mathbf{n}}$, and $d\Omega = d\theta/2\pi$.

We define two functions ϕ_s and ϕ_f that characterize the probability of generating chains at various angles when a splitting or fusion occurs. In the most general case, these may be functions of the intensities and directions of all three chains, but must include delta functions ensuring force balance and Heaviside functions $\Theta(f)$ ensuring that all force intensities are positive (all force chains in a noncohesive material must carry compressive stress, not tensile).

$$\phi_a(\mathbf{f}_1 | \mathbf{f}_2, \mathbf{f}_3) = \delta(\mathbf{f}_2 + \mathbf{f}_3 - \mathbf{f}_1) \Theta(f_1) \Theta(f_2) \Theta(f_3) \times \psi_a(\theta_1 | \theta_2, \theta_3) |\sin(\theta_2 - \theta_3)|, \quad (3)$$

where \mathbf{f} indicates the pair $(f, \hat{\mathbf{n}})$ and ψ_a is normalized such that $\int d\theta_2 d\theta_3 df_2 df_3 \phi_a = 1$. The vertical bar is used in expressing the arguments of ϕ_a and ψ_a to indicate that the first argument is associated with the minus sign in the delta function. For splittings, the first argument corresponds to the single incoming chain. For fusions, it corresponds to the single outgoing chain.

The explicit factor of $|\sin(\theta_2 - \theta_3)|$ in Eq. (3) serves several purposes. For the splitting function, it is included to remind us that ϕ_s must vanish for splitting events in which the outgoing chains are collinear and oppositely directed, as this would generate infinite force intensities. It is also reasonable to assume that splitting events with outgoing chains close to the same direction are rare, though ψ_s could of course be chosen to make such events as probable as desired. For the fusion function, the factor gives the density of intersection points per unit area for unit chain densities of chains with orientation θ_2 and θ_3 , which should clearly affect the probability of fusions occurring. This factor also simplifies the normalization of ψ_a , since for $\theta_1 = 0$ and any function A we have

$$\begin{aligned} & \int_0^\infty df_2 df_3 \delta(\mathbf{f}_2 + \mathbf{f}_3 - \mathbf{f}_1) A(f_1, f_2, f_3) \\ &= \int_0^\infty df_2 df_3 \delta(f_2 \cos \theta_2 + f_3 \cos \theta_3 - f_1) \\ & \quad \times \delta(f_2 \sin \theta_2 + f_3 \sin \theta_3) A(f_1, f_2, f_3) \\ &= \frac{1}{\sin(\theta_2 - \theta_3)} A\left(f_1, \frac{f_1 \sin \theta_2}{\sin(\theta_2 - \theta_3)}, \frac{f_1 \sin \theta_3}{\sin(\theta_2 - \theta_3)}\right). \end{aligned} \quad (4)$$

Note that ψ_a must be symmetric in its second and third arguments; in the case of splitting (fusion), switching the labels of the two outgoing (incoming) chains cannot change the physics. Note also that the delta function is really the product of two delta functions, as shown in Eq. (4), one for each component of force balance, and therefore has a dimension of inverse force squared. We will restrict our attention to homogeneous and isotropic

systems, for which ψ_a does not vary with position and depends only upon the relative angles between its three arguments.

In general, ψ_s and ψ_f are different, owing to the physical difference between splitting and fusion events. As illustrated in Fig. 1 for a particularly simple system, the type of defect required to induce splitting is not necessarily present at a fusion. The boundary conditions on the various chains involved make for different probabilities between splittings and fusions for a given local geometry of the granular packing.

The following Boltzmann equation describes the variation of $P(f, \theta, \mathbf{r})$ along the direction $\hat{\mathbf{n}}$, where λ and μ are constants required on dimensional grounds and, for notational convenience, we have dropped the \mathbf{r} from the argument of all of the P 's:

$$\begin{aligned} (\hat{\mathbf{n}} \cdot \nabla) P(\mathbf{f}) = & \frac{1}{\lambda} \left[-P(\mathbf{f}) + 2 \int df' df'' d\theta' d\theta'' \phi_s(\mathbf{f}' | \mathbf{f}, \mathbf{f}'') P(\mathbf{f}') \right] \\ & + \frac{\mu}{\lambda} \int df' df'' d\theta' d\theta'' [\phi_f(\mathbf{f} | \mathbf{f}', \mathbf{f}'') P(\mathbf{f}') P(\mathbf{f}'') \\ & - 2\phi_f(\mathbf{f}' | \mathbf{f}, \mathbf{f}'') P(\mathbf{f}) P(\mathbf{f}'')]. \end{aligned} \quad (5)$$

In this expression, all integrals over angles run from $-\pi$ to π and all integrals over forces run from 0 to ∞ . The first term on the right hand side in Eq. (5) describes the decay of force chain density in the direction of the chain due to splitting of the chain. λ thus corresponds to the average distance a chain propagates before splitting, in the absence of all other chains. In principle, λ may be a function of the direction $\hat{\mathbf{n}}$ and position, but is a single constant for homogeneous and isotropic systems. The second term on the right hand side describes the increase in $P(\mathbf{f})$ due to the splitting of other chains. The factor of two in this term is due to the fact that ϕ_s has been normalized to unity while a splitting event produces two outgoing chains. The final integral in Eq. (5) is quadratic in P and describes the effects of fusions. The quantity μ has dimensions of $1/P$, or *force* \times *length* in 2D. As with λ , we assume μ is independent of θ . The factor of 2 in arises because the chain in the θ direction can be either of the two incoming chains in a fusion.

The boundary conditions to be applied to Eq. (5) are suggested by Fig. 1. At each point on the boundary of a sample we may specify the density of ingoing chains of any intensity, but we may not specify the density of outgoing chains. This means that there is no simple way to assign boundary conditions corresponding to the overall stress on a boundary; the density of outgoing chains, which add to the normal and shear stresses just as ingoing ones do, is determined by the splittings and fusions within the sample. In the slab geometry, however, it is possible to specify the total vertical force applied to the top and bottom boundaries, due to the symmetry of the force network under multiplication of all intensities by a common factor. One may first specify the density of inward directed chains, then compute the density of outward directed chains using the Boltzmann equation, compute the

stresses at the boundary, then rescale all of the forces in the system to arrive at the desired boundary stress. Satisfying conditions on both the normal and shear stress may also require adjustment of the relative densities of chains in different inward-pointing directions. The manner in which boundary conditions on the chain densities can be specified will be clarified by the precise treatment of a special case in Section 3.

The fact that we may only specify the densities of ingoing chains at a boundary is a part of the definition of the λY -model that deserves further comment. Microscopically, when we specify that a chain of a given strength must pass through a certain point on the boundary, the boundary condition *defines* the direction of that chain to be inward. This is physically plausible because we would not expect to be able to apply a boundary condition that requires an intricate conspiracy of fusions and splittings to create a chain that propagates outward at the point in question. In the context of the Boltzmann equation, in which we do not specify individual chains but only densities, this is reflected mathematically in the fact that specification of outgoing chain densities leads to nonsense in certain generic situations, as shown in Section 3, for example.

To appreciate the meaning of the chain directions at the boundaries, it may be helpful to consider the application of force in the following way. Imagine a packing of grains between two flat plates that are perforated with holes much smaller than the grain size and held at fixed separation. Now imagine poking needles through the holes in the plates, with the force applied to each needle being specified externally and an equal total force applied from above and below. In this situation, there is a clear difference between chains that end on needles and chains that end on a contact between a grain and one of the plates. The former must be present due to the boundary conditions, and are therefore ingoing. (See Figure 2.) The latter exist only as a response to the applied forces. They would shift around if a new needle were poked in initiating a new chain and hence are not specifiable as boundary conditions. Now in the case of two rigid, smooth flat plates that are simply pushed together, it is not clear how to distinguish the ingoing from the outgoing chains. Nevertheless, for present purposes, we assume (plausibly, we think) that such a distinction is somehow embedded in whatever physics at the grain scale is responsible for the organization of stress into force chains in the first place. Exploration of the alternative hypothesis – that ingoing and outgoing chains are indistinguishable – is beyond the scope of this paper. It would require self-consistent choices of the splitting and fusion functions so as to yield structures that satisfy the same Boltzmann equation when the directions of all force chains are reversed.

2.2 Rescalings and the importance of nonlinear terms

In the isotropic Boltzmann equation, the parameter λ can be set equal to unity without loss of generality via a rescal-

ing of lengths: $x \rightarrow x/\lambda$, $z \rightarrow z/\lambda$, $P \rightarrow \lambda P$ and $\mu \rightarrow \mu/\lambda$. In these new units, μ has dimensions of force.

A crucial feature of Eq. (5) is that the fixed point solution $P(\mathbf{f}) = 0$ is unstable. Consider the total force density in the system, defined as $\mathcal{F} = \int d\mathbf{f} d\theta d\mathbf{r} f P(\mathbf{f})$. For $P(\mathbf{f}) \ll 1$, the value of \mathcal{F} is determined by the linear terms in the Boltzmann equation. But these describe only splittings, and every splitting increases \mathcal{F} since force balance requires that the sum of the two outgoing intensities be larger than the incoming intensity. If we begin with a single chain, each generation of splittings increases \mathcal{F} by a constant factor that depends upon ψ_s but is always greater than unity. In a sufficiently large sample, the rate of increase of \mathcal{F} due to splitting will exceed the rate of decrease due to leakage through the boundary. In order to regulate this divergence, the nonlinear terms must be included. This argument will be made precise for the choice of ψ_s discussed in Section 2.3 and developed in somewhat more general terms in the appendix.

The inclusion of the nonlinear terms requires the introduction of the dimensionful parameter μ . To understand how this parameter is determined, it is helpful to write it as the product of two factors, $\mu = \mu_0 Y$, where μ_0 has units of force and Y is simply a numerical constant. Since there is no intrinsic force scale in the system, μ_0 can be chosen arbitrarily without loss of generality. This freedom is a direct consequence of the fact that, given any DFCN, there exists a continuous family related to it by multiplication of all of the chain intensities by a constant factor. The rescaling associated with the choice of μ_0 is exactly compensated by a rescaling of the argument f in $P(f, \theta, \mathbf{r})$, so that the geometric structure of the DFCN is unchanged.

The factor Y is determined by the overall probability of fusions occurring when chains intersect. Y can be thought of as a normalization associated with ϕ_f . In physical terms, changes in Y have real effects on the P 's, as Y ultimately determines the density of fusions in the system. It is convenient, however, to work with variables $P' \equiv P/Y$. This results in the same Boltzmann equation with $Y = 1$, which we will work with henceforth while dropping the primes on the P 's. Thus we are left with a Boltzmann equation with no parameters other than the choices of ψ_s and ψ_f : for the purposes of mathematical analysis λ and μ can both be scaled to unity.

Eq. (5), with λ and μ both scaled to 1, but with generic forms of ψ_s and ψ_f , has proven difficult to solve for even the simplest sample geometries and boundary conditions (though the authors still hold onto hope for further analysis). Moreover, the numerical generation of directed force chain networks encounters serious difficulties for systems deep enough that the nonlinear processes become important. Useful insights can be obtained, however, by considering some special cases where analytical progress is possible.

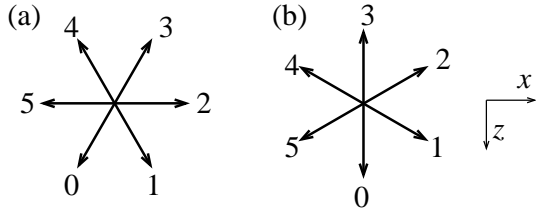


Fig. 3. Two choices of the discrete set of six permitted directions of force chains.

2.3 A solvable case: 120° splittings and fusions

We now consider a system for which

$$\psi_{s,f}(\theta_1 | \theta_2, \theta_3) = \frac{1}{2} \left[\delta(\theta_{21} - \frac{\pi}{3}) \delta(\theta_{31} + \frac{\pi}{3}) + \delta(\theta_{21} + \frac{\pi}{3}) \delta(\theta_{31} - \frac{\pi}{3}) \right], \quad (6)$$

where $\theta_{ij} \equiv \theta_i - \theta_j$. This corresponds to the case where both splittings and fusions are always symmetric and form vertices composed of 120° angles, as in Fig. 1. Note that in this case, chains with different intensities or with directions that are not parts of the single symmetric star of six unit vectors, cannot interact via fusion. So we further assume that all chains initiated at the boundary have directions chosen from a single “6-fold star” and have identical intensities f_* :

$$P(f, \theta) = \sum_{n=0}^5 P_n \delta(f - f_*) \delta(\theta - \theta_n), \quad (7)$$

where $\theta_n \equiv (n - 1/2)\pi/3$ as illustrated in Fig. 3(a). We refer to this orientation of the 6-fold star vectors as “horizontal”, since it includes directions oriented horizontally. Another choice we have studied extensively is the “vertical” orientation shown in Fig. 3(b). It turns out that for the horizontal orientation, exact analytical expressions are easier to obtain, but the response functions (computed numerically for the vertical orientation) are qualitatively similar.

For the horizontal orientation, Eq. (5) reduces to

$$\hat{\mathbf{v}}_i \cdot \nabla P_i = -P_i + P_{i+1} + P_{i-1} + (P_{i+1}P_{i-1} - P_iP_{i+2} - P_iP_{i-2}), \quad (8)$$

where all indices are taken modulo 6 and $\hat{\mathbf{v}}_i \equiv (\cos \theta_i, \sin \theta_i)$. Note that all integrations over f and θ have been performed, and the only remaining difference between the coefficients of splitting and fusion events is the factor Y , which has been absorbed into the P ’s.

The restriction of the possible orientations of force chains to six directions does *not* imply that the chains reside on a regular geometric lattice. The splitting and fusion events occur at arbitrary positions, governed only by the probabilistic rules encoded in the Boltzmann equation.

3 Horizontally uniform solutions

Let us now construct solutions of Eq. (8) for the case of an infinite horizontal slab subject to a horizontally uniform load. Let $z = 0$ represent the top surface of the slab and $z = d$ the bottom. For simplicity, we consider the case where the loading (and hence the full solution) is symmetric under reflection through a vertical line, as well as translationally invariant in the horizontal direction. Thus we have $P_0 = P_1$, $P_5 = P_2$, and $P_4 = P_3$ at all points in the system and $\partial_x P_n = 0$ for all n .

The Boltzmann equation then reduces to the following set:

$$\frac{\sqrt{3}}{2} \partial_z P_1 = P_2 - P_1 P_3, \quad (9)$$

$$P_2 = P_1 + P_3 + [P_1 P_3 - P_2(P_1 + P_3)], \quad (10)$$

$$-\frac{\sqrt{3}}{2} \partial_z P_3 = P_2 - P_1 P_3, \quad (11)$$

where each of the P ’s is a function of z alone. From Eqs. (9) and (11), one sees immediately that $G \equiv P_1 + P_3$ is a constant (determined by the boundary conditions), and from Eq. (10) we have

$$P_2 = \frac{G + P_1 P_3}{1 + G}. \quad (12)$$

Substituting into Eqs. (9) and (11) leads to the two coupled ordinary differential equations for $P_1(z)$ and $P_3(z)$:

$$\begin{aligned} \frac{dP_1}{dz} &= \frac{2G}{(1+G)\sqrt{3}} (1 - P_1 P_3) \\ \frac{dP_3}{dz} &= \frac{-2G}{(1+G)\sqrt{3}} (1 - P_1 P_3). \end{aligned} \quad (13)$$

These equations are to be supplemented with boundary conditions on P_1 at $z = 0$ and on P_3 at $z = d$. (P_1 and P_3 are the densities of downward and upward directed chains, respectively.) From Eq. (2), the stress components are simply

$$\sigma_{zz} = \frac{3}{2}(P_1 + P_3), \quad (14)$$

$$\sigma_{xx} = 2P_2 + \frac{1}{2}(P_1 + P_3), \quad (15)$$

$$\sigma_{xz} = 0. \quad (16)$$

Before proceeding to the full solution of Eqs. (13), it is instructive to consider the linearized theory in the vicinity of $P_i = 0$:

$$\partial_z P_1 = \frac{2}{\sqrt{3}}G; \quad \partial_z P_3 = \frac{-2}{\sqrt{3}}G. \quad (17)$$

Since $G \equiv P_1 + P_3$ is a positive constant, one sees immediately that P_3 will become negative for sufficiently large z . In fact, for arbitrarily large values of $P_3(0)$, one sees immediately that $P_3(d)$ must become negative for $d > \sqrt{3}/2$, since the smallest possible value of G is $P_3(0)$. Thus the

linear theory produces unphysical results for systems of dimensionful depth $\lambda\sqrt{3}/2$ or greater. The problem can be traced to the divergence of chain densities mentioned above that occurs when the system is sufficiently deep to allow an appreciable number of force chains to “turn around”.

In marked contrast to the linear theory, the full theory expressed in Eq. (13) admits physical solutions for all possible specifications of $P_1(0)$ and $P_3(d)$ for arbitrarily large d . Let B denote $P_1(0)P_3(d)$. The solutions are

$$P_1 = \begin{cases} \frac{G}{2} - \gamma_+ \tanh \left[\frac{2}{\sqrt{3}} \frac{G\gamma_+}{(1+G)} (z - C) \right] & G > 2, B > 1 \\ \frac{G}{2} - \gamma_+ \coth \left[\frac{2}{\sqrt{3}} \frac{G\gamma_+}{(1+G)} (z - C) \right] & G > 2, B < 1 \\ \frac{G}{2} + \gamma_- \tan \left[\frac{2}{\sqrt{3}} \frac{G\gamma_-}{(1+G)} (z - C) \right] & G < 2 \end{cases} \quad (18)$$

where $\gamma_{\pm} \equiv \sqrt{\pm(G^2 - 4)}/2$ and G and C are constants determined by the specification of $P_1(0)$ and $P_3(d)$.

We will see below that a solution with non-negative densities exists for arbitrary choices of $P_1(0)$ and $P_3(d)$ and arbitrary values of d . On the other hand, for choices of $P_3(0)$ and/or $P_1(d)$ within some ranges, the equations lead to negative densities or no solutions at all. This is a mathematical expression of the physically plausible statement that one cannot specify in advance the densities of chains directed outward from boundary.

Exactly which specification of $P_1(0)$ and $P_3(d)$ correspond to a given physical situation is not entirely clear. For a slab squeezed between two plates, however, a natural assumption is that the boundary conditions should be symmetric: $P_3(d) = P_1(0)$. In this case, $C = d/2$. Two particular solutions for symmetric boundary conditions are shown in Fig. 4. Part (a) shows the case $G > 2$, which yields extended flat regions in the upper and lower halves of the slab that are connected by a transition region. The flat regions correspond to a uniform stress that is anisotropic: $\sigma_{xx} \neq \sigma_{zz}$. The width of the transition region is of order λ , with an exponentially fast approach to the plateaus on either side. Surprisingly, the transition region is marked by a strong variation in the horizontal stress. Though the effect of such a transition region on the dynamical properties of the system is far from clear, it is interesting to note that the theory gives rise to a localized inhomogeneity that could influence shear band formation. The increased horizontal stress in the transition region can be intuitively understood by considering a case of very large $P_1(0)$ and $P_3(d)$. In such a case, nearly all the chains in the top half of the sample are downward pointing, and nearly all the chains in the bottom half are upward pointing. The density of horizontal chains is determined by the splitting length, λ . In the transition region, however, there is a high density of intersections of upward and downward pointing chains, which result in fusions that generate horizontal chains. Hence the density of horizontal chains is higher in the transition region, being determined by the distances chains propagate before fusing, rather than the longer distance required for splitting.

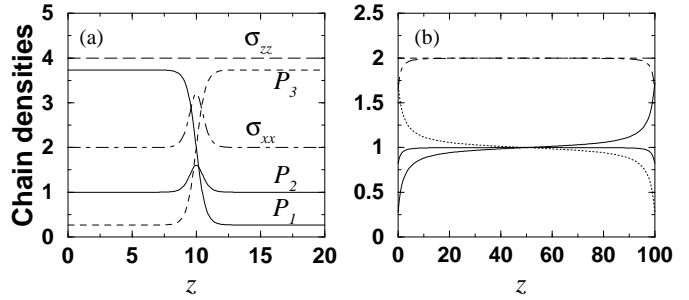


Fig. 4. Typical solutions of the discrete Boltzmann equation with symmetric boundary conditions. (a) A generic solution with an exponentially localized transition region in the middle of the slab. (b) A solution with power-law boundary layers and a plateau in the middle, corresponding to $P_1 + P_3 = 2 - \epsilon$.

Fig. 4(b) shows density profiles for $G < 2$. In this case, it is the edges that deviate from the fixed point plateau in the middle, but the approach to the fixed point is a power law, $\sim 1/z$, so one cannot clearly define a boundary layer.

The complete structure of the solution space is displayed in Fig. 5. All points with $P_1P_3 = 1$, shown as a thick dotted line, are fixed points. Since $P_1 + P_3$ is a constant, each trajectory is a line with slope -1 . The arrows indicate the direction in which the systems moves with increasing z . For trajectories in the region above the fixed line, P_1 decreases with depth and P_3 increases, and vice-versa for trajectories below (or to the left of) the fixed line. For small systems, trajectories in the lower left corner, near the origin, may be relevant. For deep systems, however, the relevant trajectories must be ones that pass very close to some fixed point where P_1 and P_3 can stay nearly stationary for a long “time”.

Let us now consider the possibilities for satisfying various boundary conditions. Let U be the “starting” point $(P_1(0), P_3(0))$ and V be the “ending” point $(P_1(d), P_3(d))$. First, we show that for any d , any $P_1(0)$, and any $P_3(d)$, U can be chosen in the first quadrant in such a way that V lies in the first quadrant; i.e., there exists a trajectory with no negative chain densities that satisfies the boundary conditions. To see this, first note that $P_1(d)$ can never be negative. If U is chosen below the fixed line, P_1 always increases with increasing z . On the other hand, since trajectories can never cross the fixed line, if U is above the fixed line, the entire trajectory is confined to the first quadrant. To complete the proof, it is sufficient to show that as U varies in the first quadrant along the vertical line corresponding to any given choice of $P_1(0)$, $P_3(d)$ takes on all possible positive values. Consider $U = (x, y)$. For any nonzero value of d , $P_3(d)$ is negative for $y = 0$, since all trajectories beginning on the x -axis pass immediately into the fourth quadrant. As y is increased toward the fixed point $y = 1/x$, $P_3(d)$ rises continuously to $1/x$. As y is increased beyond $1/x$, $P_3(d)$ increases without bound. Hence, given $P_1(0) = x$ one can always choose y such that $P_3(d)$ has any specified positive value. Fig. 5(b) indicates

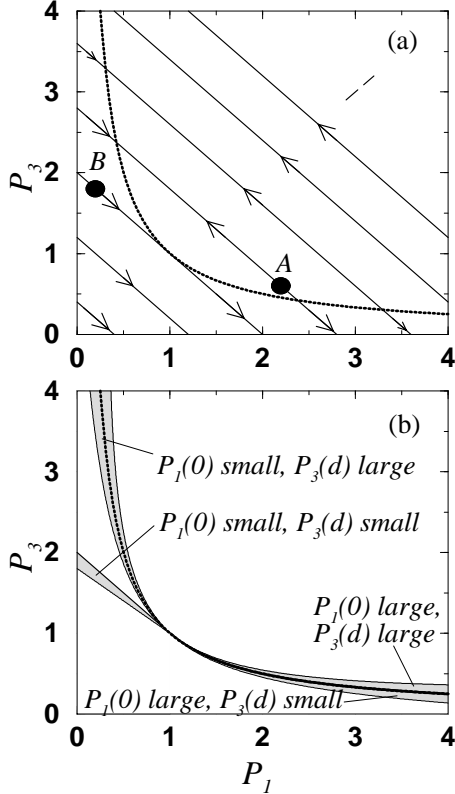


Fig. 5. (a) Trajectories of Eq. (13) in the P_1 - P_3 plane. The curved line, $P_1P_3 = 1$ is a set of fixed points. The diagonal lines indicate the trajectories, with the arrows showing the direction of flow with increasing z . For systems deeper than λ , the typical length a force chain propagates before splitting, trajectories must either start very close to the line of fixed points (e.g. at point B), or on a trajectory that will take the system close to a fixed point (e.g. at point A). (b) The shaded regions indicate where trajectories must start in order to satisfy various possible boundary conditions for deep systems. The starting points must lie either in the vicinity of the fixed line, or just below the line of slope -1 tangent to the fixed line. For $P_1(0)$ small and $P_3(d)$ large, the starting point may be on either side of the fixed line.

roughly where U must be chosen in order to satisfy various boundary conditions when d is large. For d small or of the order of unity, the trajectories generally lie completely within the unshaded regions of the diagram.

Suppose now that we attempt to specify P_1 and P_3 at the top boundary. In other words, we specify U completely. In this case, problems arise for sufficiently large d whenever U is below the fixed line for $P_1(0) > 1$ or below the line $P_1 + P_3 = 2$ for $P_1(0) < 1$. Each trajectory in these regions passes into the fourth quadrant at some finite value of z , generating the unphysical result that P_3 becomes negative. Similar difficulties arise if one attempts to specify V rather than U . Finally, if one attempts to specify $P_1(d)$ and $P_3(0)$, there are no solutions at all for d large and $P_1(d) > P_3(0) + 1/P_3(0)$. The fact that certain regimes are prohibited in each of these cases is consistent

with the assertion that physical constraints permit the specification of $P_1(0)$ and $P_3(d)$ only.

For deep systems (large d), there are three types of typical solutions, corresponding to the three expressions in Eq. (18):

Type I: $P_1(0) > 1$ and $P_1(0)P_3(d) > 1$. The motion must take place in the region above the line of fixed points, starting close to the line, at a point such as A in Fig. 5. For symmetric boundary conditions, the motion will also end near a fixed point, producing the behavior shown in Fig. 4(a).

Type II: $P_1(0) > 1$ and $P_1(0)P_3(d) < 1$. The motion takes place in the lower right portion of the plane. The trajectory must start just below a fixed point. Such solutions occur if the bottom boundary condition is taken to be $P_3(d) = 0$. Following such a trajectory backwards (up from the bottom of the sample) one finds the densities approach their fixed point values like $1/z$. We will not pursue this case further here, but note that related asymmetric solutions might be relevant when gravity is included in the model.

Type III: $P_1(0) < 1$ and $P_3(d) < 1$. For large d , the motion must take place on a trajectory just below the one marked B in Fig. 5, so as to pass very close to the fixed point at $P_1 = P_3 = 1$. The density profiles associated with these trajectories are similar to those of Type II, but show increasing deviations from the fixed point values at both the top and bottom of the slab. Density profiles for a Type III solution are shown in Fig. 4(b). (Note the difference in horizontal scale between parts (a) and (b).) Though these solutions are mathematically consistent, they have the counter-intuitive physical property that the density of upward-pointing chains at the top surface is larger than the imposed density of downward-pointing chains.

All other solutions are related to these three types by reflection through $z = d/2$ and interchange of P_1 and P_3 .

For deep systems, the system is primarily composed of regions in which (P_1, P_3) lies close to a fixed point. The nature of the directed force chain networks at the different fixed points is therefore of interest. First, we note that the networks associated with generic fixed points are anisotropic, having different densities for chains in different directions. Letting p designate the value of P_1 at a fixed point, the value of P_3 at that fixed point is $1/p$. We emphasize that this is not a result of intrinsic anisotropy in the material, but rather a result of the boundary conditions. The situation is similar to that of an elastic material that may be isotropic when unloaded, but becomes anisotropic when subjected to a uniaxial stress. There is a crucial difference, however, in that the force chain network has no stable unloaded state. Thus, except under conditions of pure hydrostatic pressure, the response of the force chain network to perturbations in its loading will generally be anisotropic. The exceptional case is the fixed point at $p = 1$, where the system is indeed isotropic.

Second, we may compute two distinct quantities that might be thought of as analogous to the Poisson ratio of standard elasticity theory. The first is the ratio $\Delta\sigma_{xx}/\Delta\sigma_{zz}$

obtained upon increasing the strengths of the forces in all of the force chains. Since this does not change the network at all, the resulting ratio is just equal to σ_{xx}/σ_{zz} at the fixed point. Using Eq. (14), we find

$$\nu_1 \equiv \frac{\sigma_{xx}}{\sigma_{zz}} = \frac{4 + p + p^{-1}}{3(p + p^{-1})}, \quad (19)$$

which varies monotonically from 1 at $p = 1$ to $1/3$ for $p \rightarrow \infty$.

The other quantity analogous to the Poisson ratio is obtained by considering small increases in the applied *density* of force chains, rather than their strengths. In this case, the system moves along the line of fixed points and we calculate

$$\nu_2 \equiv \frac{\partial_p \sigma_{xx}}{\partial_p \sigma_{zz}} = 1/3. \quad (20)$$

It is amusing to note that a Poisson ratio of $1/3$ arises also in studies of ball-and-spring networks with energies expressible as a sum of two-body central forces.[18] We shall see in Section 5.1, however, that this feature is specific to the horizontal orientation of the 6-fold star vectors. For the vertical orientation, ν_2 varies with p .

It is also interesting to note that ν_1 and ν_2 lie within the range of stability for 2D isotropic elasticity, in contrast to the Poisson ratio computed in Ref. [16] from the linear theory of DFCN's. This is an indication that there are significant differences between the elasticity theories in the vicinity of a nontrivial fixed point and that obtained in the vicinity of the origin.

4 Response to a localized force

The response of the directed force chain network to a localized force applied at the top boundary may be computed via linearization about the appropriate fixed point. In general, for a DFCN with a continuum of force chain intensities, there are two distinct ways to apply a localized perturbation: (1) by changing the strength of some of the force chains injected at the boundary; or (2) by adding some new force chains of chosen intensities. In the case where splitting and fusion angles are always 120° , however, option (1) is not available. Because ψ_s and ψ_f permit interactions only among force chains of the same intensity, increasing the strength of one chain would be equivalent to removing that chain from the existing network and creating an entirely new network completely decoupled from the original, which would lead right back to the problem of the failure of the linear theory in the vicinity of the origin. Thus we must consider option (2), in which we inject a low density of new force chains with intensity f_* along one or more of the directions $\hat{\mathbf{v}}_i$.

In the fixed point DFCN, the chain densities are translationally invariant. This permits the derivation of decoupled equations for the different Fourier modes of a perturbation applied at the top surface. We begin from the six equations obtained from Eq. (8):

$$\frac{\sqrt{3}}{2} \partial_z P_1 + \frac{1}{2} \partial_x P_1 = -P_1 + P_2 + P_0$$

$$+ (P_0 P_2 - P_1 P_3 - P_1 P_5), \quad (21)$$

$$\partial_x P_2 = -P_2 + P_3 + P_1 \\ + (P_1 P_3 - P_2 P_4 - P_2 P_0), \quad (22)$$

$$\frac{-\sqrt{3}}{2} \partial_z P_3 + \frac{1}{2} \partial_x P_3 = -P_3 + P_2 + P_4 \\ + (P_2 P_4 - P_3 P_5 - P_3 P_1), \quad (23)$$

and similar equations for P_4 , P_5 , and P_0 . Fixed point solutions of these equations have the form $(P_1^0, P_3^0, P_4^0, P_0^0) = (p, 1/p, 1/p, p)$, with $P_2^0 = P_5^0$ given by Eq. (12). Let $p_n = P_n(x, z) - P_n^0(x, z)$ be the deviations from the fixed point and define Fourier coefficients $Q_n(q, z)$ via

$$p_n = \int_{-\infty}^{\infty} dq Q_n(q, z) e^{iqx}. \quad (24)$$

Linearization of Eq. (21) in Q yields

$$\frac{d}{dz} \mathbf{Q}(q) = \mathbf{M}(q) \cdot \mathbf{Q}(q), \quad (25)$$

where \mathbf{Q} is the column vector (Q_1, Q_3, Q_4, Q_0) and the complex elements of \mathbf{M} are complicated algebraic functions of p and q . Analytic expressions for the eigenvalues of \mathbf{M} may be obtained, but they are exceedingly complicated functions of p and q and we do not reproduce them here. (They involve solutions of quartic equations whose coefficients are polynomials of seventh order in p and third order in q .) The eigenvalues and eigenvectors of $\mathbf{M}(q)$ and $\mathbf{M}(-q)$ are related by the condition that the response to a real perturbation must be real.

To compute the response to a localized perturbation applied at the top of a semi-infinite system, we seek solutions for which all Q_n 's vanish as $z \rightarrow \infty$. The symmetry of the Boltzmann equation and the fixed point solution under $x \rightarrow -x$ guarantees that for every complex eigenvalue κ of $\mathbf{M}(q)$, there will be a complex conjugate partner κ^* . In addition, though the $z \rightarrow -z$ symmetry is broken by the fixed point solution (since $P_1^0 \neq P_3^0$), there are two eigenvalues with negative real part for each q and two with positive real part. In constructing the perturbation, the coefficients of all eigenvectors having eigenvalues with positive real parts must be zero, since for these modes the Q_n 's grow exponentially with increasing z . By taking appropriate linear combinations of the eigenvectors associated with the eigenvalues that have negative real parts, one can arrange to satisfy any specified boundary condition on $p_1(x, 0)$ and $p_0(x, 0)$. Note that $p_3(x, 0)$ and $p_4(x, 0)$ are then determined, which is consistent with the general rule that we may specify the densities of inward-directed chains only.

For simplicity, we restrict the presentation here to applied perturbations that are symmetric under reflection about a vertical line: perturbations with $p_0(x) = p_1(-x)$. The general form of the solution for $\mathbf{p} = (p_1, p_3, p_4, p_0)$ is then

$$\mathbf{p}(x, z) = \int_0^{\infty} dq \sum_{j=1}^2 a_j(q) e^{\text{Re}[\kappa_j]z} \cos(qx - \text{Im}[\kappa_j]z) \mathbf{e}_j, \quad (26)$$

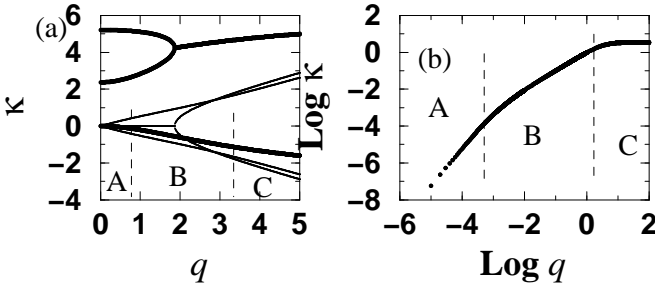


Fig. 6. The spectrum of eigenvalues of the linear operator governing perturbations in the vicinity of a fixed point for the case of the horizontal orientation of 6-fold star vectors. (a) The case $P_1 = 3$. Thick (thin) lines are the real (imaginary) parts of κ . A, B, and C mark regimes corresponding to different behavior of the response function. (See text.) (b) The case $P_1 = 1.001$. Only the real part of κ is shown. The quadratic, linear, and flat behaviors in the regimes A, B, and C are clearly visible.

where κ_j is an eigenvalue with negative real part, \mathbf{e}_j is its associated eigenvector, and $a_j(q)$ is a constant determined by the boundary conditions.

Fig. 6(a) shows the eigenvalues $\kappa(q)$ of \mathbf{M} , computed for the case $p = 3$. The thick lines indicate the real parts of κ and the thin lines the imaginary parts. The lower thick line and the two thin lines that emerge from the origin above and below the axis correspond to a complex conjugate pair of roots, the two roots with negative parts and therefore the only ones relevant for the response in a semi-infinite system. The spectrum may be divided, roughly, into three regions. In region A, corresponding to the smallest values of both q and $|\text{Re}[\kappa]|$, neglecting all terms of order q^3 or higher in \mathbf{M} we find

$$\kappa \approx -Dq^2 + icq, \quad (27)$$

where c and D are real constants:

$$D = \frac{4}{\sqrt{3}} \frac{1}{(p^2 - p^{-2})};$$

$$c = \frac{1}{\sqrt{3}}. \quad (28)$$

There is a transition region B with intermediate q and $|\text{Re}[\kappa]|$, and finally, region C, a plateau in $|\text{Re}[\kappa]|$ for large q .

The response at large z is dominated by the slowest decaying modes, those with $|\text{Re}[\kappa]|$ closest to zero. From the observation that there are no values of q other than zero for which $\text{Re}[\kappa]$ vanishes, it is clear that these are the long wavelength modes with the disperion relation of Eq. (27). Thus for large z we can approximate the integral in Eq. (26) by

$$\mathbf{p} \sim \int_0^\infty dq e^{-Dzq^2} [\cos(q(x - cz))\mathbf{e}_1 + \cos(q(x - cz))\mathbf{e}_2] \quad (29)$$

$$\sim z^{-1/2} \left[e^{-\frac{(x-cz)^2}{4Dz}} \mathbf{e}_1 + e^{-\frac{(x+cz)^2}{4Dz}} \mathbf{e}_2 \right]. \quad (30)$$

The response at large depths consists of two Gaussian peaks that propagate away from $x = 0$ at an angle of $\tan^{-1} c$ and have widths proportional to \sqrt{Dz} .

Eq. (28) indicates that c corresponds to angles of propagation along the directions $\hat{\mathbf{v}}_1$ and $\hat{\mathbf{v}}_0$ for all of the fixed points. This appears to be special to the horizontal orientation of the star vectors. (See Section 5.1 below.) D diverges as the isotropic fixed point, $p = 1$, is approached. This means that for nearly isotropic fixed points, the peaks at large z become increasingly broad. In addition, the region over which the spectrum is quadratic (region A), becomes smaller and smaller, so that the emergence of the two peaks occurs only for exceedingly large z . Fig. 6(b) shows the real part of the spectrum for the case $p = 1.001$, plotted on a logarithmic scale. In this case we see that the transition region B is a clearly defined regime of linear dispersion. Linear dispersion generally implies either a single, centered peak in the response, or propagating peaks that broaden linearly with depth.

The full response to a localized applied force can be computed numerically. Fig. 7 shows the response function for the case $p = 3$. The curves were obtained by approximating the integral over q in Eq. (26) with a sum over discrete values $q = (n - 1/2)\delta q$, with $\delta q = 0.01$ and $1 \leq n \leq 1000$. This range of q 's contains enough high q 's to construct a relatively sharp initial Gaussian at $z = 0$, and enough low q 's to observe the response at large z . For each q , the eigenvalues and eigenvectors of \mathbf{M} are determined. We then obtain the linear combination of the two stable eigenvectors required to produce the vector $\mathbf{Q} = (1, y, y, 1)$, where y is unspecified. (The two conditions $p_1(q) = 1$ and $p_0(q) = 1$ determine the linear combination of the two eigenvectors completely, and hence determine $p_3 = p_4 = y$, and p_2 and p_5 in turn.) These linear combinations of eigenvectors are then multiplied by a factor ($a_j = \exp(-q^2/10)$) so that the sum in Eq. (26) at $z = 0$ yields centered Gaussians for p_1 and p_0 , which constitute the applied perturbation. The response is then determined at various values of z by summing the integrand of Eq. (26) over the discrete set of q 's.

Fig. 7(a) shows the p_n 's at the top surface. The identical, centered Gaussian p_1 and p_0 represent the imposed boundary condition. The other p_n 's at the top surface are part of the response, as determined by the condition that p_3 and p_4 must vanish at $z = \infty$. Part (b) shows profiles of σ_{zz} along horizontal slices at various values of z . The curves have been scaled so that the trend toward diffusively broadening, linearly propagating peaks is evident. At large z , the peaks in this figure would become increasingly sharp while maintaining their same amplitude and position. Part (c) shows the relation of the various stress components at large z .

5 Other choices of star vectors

5.1 6-Fold star in the vertical orientation

After the horizontal orientation of the 6-fold set of star vectors, the next simplest case is the vertical orientation

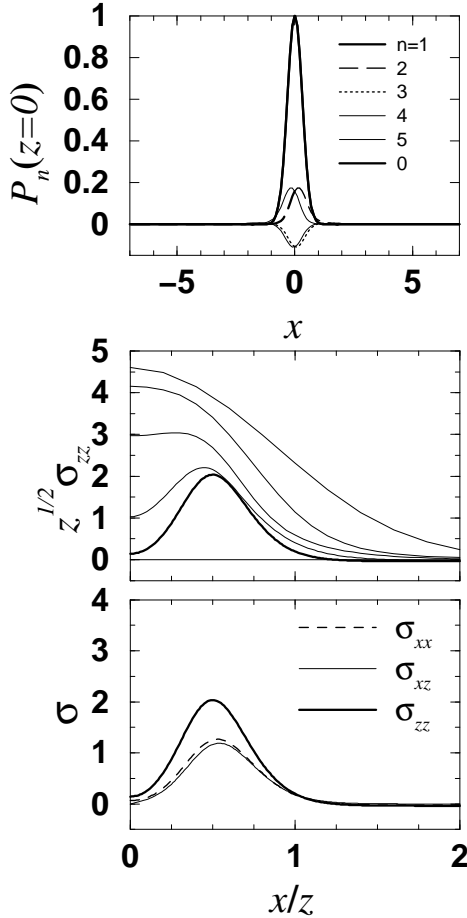


Fig. 7. Response functions for 6-fold star vectors in horizontal orientation. (a) P_n 's at the top surface. P_1 and P_0 are identical and are specified as boundary conditions. The other P_n 's are part of the response. Due to the symmetry of the boundary conditions, $P_4(x) = P_3(-x)$ and $P_5(x) = P_2(-x)$. (b) Scaled profiles of σ_{zz} for several values of z . From top to bottom, the curves correspond to $z = 0.2, 0.5, 1, 2, 5$, and 10 . (c) Different components of the stress tensor at $z = 10$, corresponding to the thick line (b). Only positive x is shown. The symmetry of the boundary conditions implies $\sigma_{zz}(x) = \sigma_{zz}(-x)$, $\sigma_{xx}(x) = \sigma_{xx}(-x)$, and $\sigma_{xz}(x) = -\sigma_{xz}(-x)$.

of the 6-fold star. Calculations for the vertical orientation are an important means of testing the robustness of several features of the solutions found above. For horizontally uniform systems with reflection symmetry under $x \rightarrow -x$, the Boltzmann equation reduces to a set of four coupled, nonlinear, ordinary differential equations for the variables P_0 , P_1 , P_2 , and P_3 . (See Fig. 3.) Using the fact that σ_{zz} is conserved, these can be reduced to a set of three. Exact analytical solution for the chain densities as a function of depth for generic boundary conditions is difficult. Nevertheless, it is easy to find a line of fixed points, which is all that is required for carrying out an analysis of the response as performed above for the case of the horizontal 6-fold star. The fixed points identified below were found

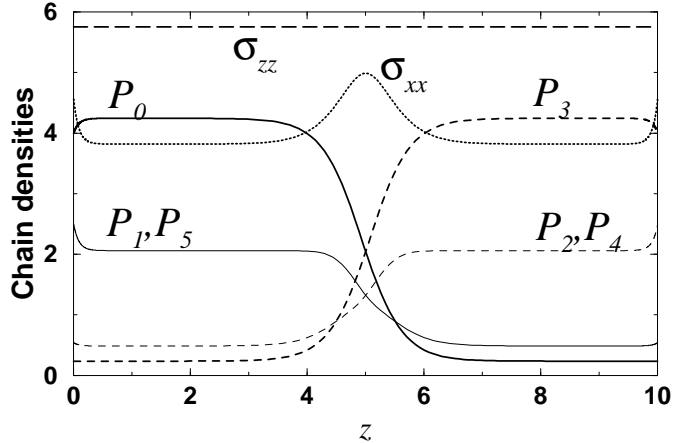


Fig. 8. A typical solution of the discrete Boltzmann equation with symmetric boundary conditions for the vertical orientation of 6-fold star vectors. (Compare to Fig. 4). The boundary conditions are $P_0(0) = 4$, $P_1(0) = P_5(0) = 2.5$, $P_3(d) = 4$, $P_2(d) = P_4(d) = 2.5$, with $d = 10$. The transition region in the middle creates a bump in σ_{xx} . Boundary layers are also present.

by making the assumption that the densities of chains in opposite directions are related by multiplicative inversion; i.e., $P_0P_3 = P_1P_4 = P_2P_5 = 1$. (This was inspired by the horizontal case, in which exactly analogous relations were found to hold, but we have not ruled out the possibility that other fixed points exist.)

Numerical solution of the two-point boundary value problem yields solutions of the type shown in Fig. 8. The basic features of the solution are quite similar to those for the horizontal orientation of the star vectors. In particular, there are flat regions corresponding to fixed point solutions and a transition region in the middle of the slab with enhanced horizontal stress. In the vertical case, however, boundary layers at the top and bottom appear as well. These arise because the additional dimensions in P -space allow for trajectories that begin away from the fixed line, approach it rapidly, then eventually diverge from it again; i.e., the fixed line has both attracting and repelling directions. The precise forms of the chain density profiles in the boundary layers and in the transition region are sensitive to the details of the imposed boundary conditions, but the enhancement of σ_{xx} in the transition region is a robust feature.

The fixed points of Eq. (8) with $x \rightarrow -x$ symmetry have

$$P_0 = p^2; P_1 = p; P_2 = p^{-1}; P_3 = p^{-2}, \quad (31)$$

which yield

$$\nu_1 = \frac{3(p + p^{-1})}{2(p^2 + p^{-2}) + (p + p^{-1})}, \quad (32)$$

$$\nu_2 = \frac{3}{1 + 4(p + p^{-1})}. \quad (33)$$

for the two types of “Poisson ratio”. Here, as for the case of the horizontal orientation of the 6-fold star vectors, ν_1

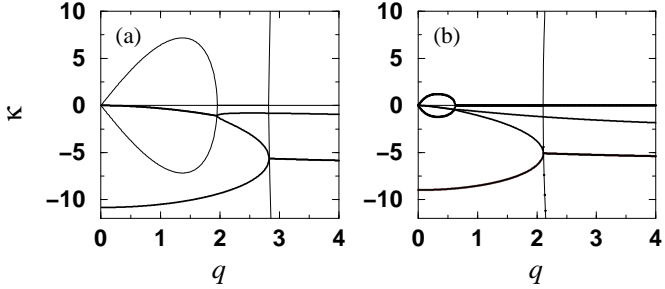


Fig. 9. The spectrum of eigenvalues of the linear operator governing perturbations in the vicinity of a fixed point for the case of the vertical orientation of 6-fold star vectors. Only the eigenvalues with negative real parts are shown. (a) The case $P_1 = 2$. Thick (thin) lines are the real (imaginary) parts of κ . (b) The case $P_1 = 1.1$. In both (a) and (b), the magnitudes of the imaginary parts have been multiplied by 15 for clarity.

varies monotonically from unity to 0 as p ranges from 1 (the isotropic fixed point) to ∞ . Unlike the horizontal case, however, ν_2 is not constant. It is again $1/3$ at the isotropic fixed point, but decreases monotonically to zero for large p .

To determine the response function, we work in the vicinity of a generic fixed point, neglecting the effects produced by the boundary layer. Fourier analysis of the linearized equations yields the spectrum shown in Fig. 9. The spectrum at low q has the form of Eq. (27), with

$$D = \frac{6(2r_{4+} + r_{3+} + 8r_{2+} + 9r_{1+} + 14)}{(4r_{1+} + 1)^2(2r_{3-} + r_{2-} - 2r_{1-})},$$

$$c = \sqrt{3}(4r_{1+} + 1)^{-1}. \quad (34)$$

where we have defined $r_{n\pm} \equiv p^n \pm p^{-n}$. For strongly anisotropic fixed points (i.e., large p) we have $c \approx (3/8)p^{-1}$ and $D \approx (4p/3)^{-1/2}$, implying, at large z , slowly diffusing peaks propagating close to the vertical direction. For nearly isotropic fixed points $p = 1 + \epsilon$, we have $c \approx \sqrt{1/3}(1 - 2\epsilon^2/9)$ and $D \approx (1/3)\epsilon^{-1}$, implying rapidly broadening peaks propagating along directions close to halfway between the star vectors. Thus, in contrast to the case of the horizontal star orientation, the direction of propagation of the peaks varies continuously from 30° near the isotropic fixed point to near 0° at the strongly anisotropic fixed points: the direction of propagation of the peaks is *not* tied to the star vector directions.

As in the case of the horizontal orientation, the region in q space over which the dispersion relation is quadratic shrinks to zero as the isotropic fixed point is approached. We also note that near the isotropic fixed point, where D becomes large, we can eliminate ϵ to obtain $c \approx \sqrt{1/3}(1 - (2/81)D^{-2})$, whereas for the strongly anisotropic fixed points, where D is small, we can eliminate p to obtain $c \approx D^2/2$. These relations between propagation direction and diffusion rate differ markedly from relations obtain from models in which the characteristic propagation direction and diffusion rates are both controlled by a parameter corresponding to the strength of the disorder, where one

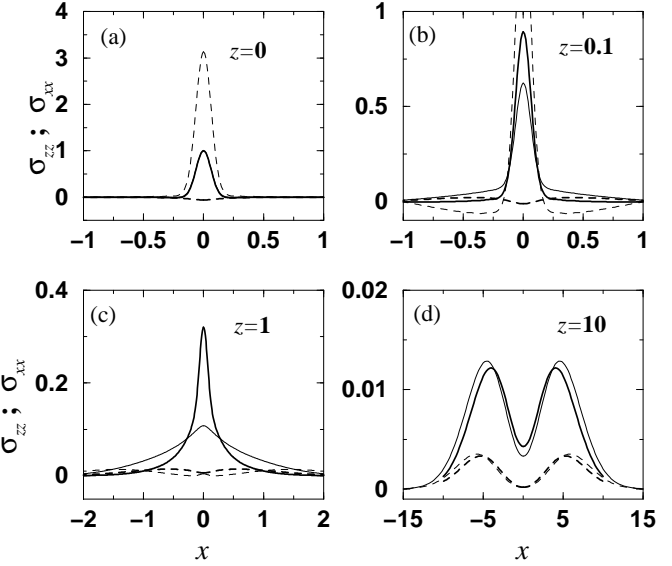


Fig. 10. Response functions for 6-fold star vectors in vertical orientation. Solid lines indicate σ_{zz} and dashed lines σ_{xx} . Thick lines correspond to a boundary condition in which P_0 is a Gaussian of unit strength and P_1 and P_5 are 0. Thin lines correspond to a boundary condition in which $P_0 = 0$ and P_1 and P_5 are Gaussian of strength 2, so as to make $\sigma_{zz}(z = 0)$ the same for both cases. Note the difference in both horizontal and vertical scales in the different panels.

finds $c \approx c_0 - aD^\alpha$ with $\alpha > 0$. [4,19] This suggests that the DFCN is *not* in the weak disorder regime.

Typical response functions are shown in Fig. 10. Two independent choices for the application of a localized vertical load are shown:

$$(p_0, p_1, p_5) = \begin{cases} (\epsilon, 0, 0) \exp(-(x/0.09)^2) & \text{and} \\ (0, 2\epsilon, 2\epsilon) \exp(-(x/0.09)^2) & \end{cases}. \quad (35)$$

These two choices produce the same profile for $\sigma_{zz}(0)$, but different profiles for $\sigma_{xx}(0)$, as shown in (a). At the small depth shown in (b), the two give different responses with somewhat complicated structures. At the intermediate depth shown in (c), the responses differ as well, but both have something like the Lorentzian structure familiar from the response of semi-infinite, standard elastic materials.[20] In particular, both show a central peak with long tails. It is not until we reach depths significantly larger than λ (which has been scaled to unity), as in (d), that we see the two diffusively broadening Gaussian emerge and the responses become quite similar.

In the asymptotic regime at large depths, Fig. 10 suggests that σ_{xx} becomes proportional to σ_{zz} . In fact, we can show both that $\sigma_{xx} \approx c^2\sigma_{zz}$ and that $c = \sqrt{\nu_2}$ by considering the eigenvectors at low q associated with the dominant branch of the spectrum. Let

$$\sigma_{xx}(q) = \mathbf{S}^{(2)} \cdot \mathbf{e}(q),$$

$$\sigma_{zz}(q) = \mathbf{C}^{(2)} \cdot \mathbf{e}(q); \quad (36)$$

where $\mathbf{C}^{(2)}$ and $\mathbf{S}^{(2)}$ are row vectors with components $\cos^2(\pi j/3)$ and $\sin^2(\pi j/3)$, respectively, and $\mathbf{e}(q)$ is the eigenvector of $\mathbf{M}(q)$ associated with the dominant branch. $\mathbf{e}(q)$ converges as q approaches zero precisely to the $q = 0$ mode corresponding to shifts along the fixed line. But these shifts are just the ones used to compute ν_2 . Thus as z increases and the surviving modes have q 's closer to zero, and the ratio $\sigma_{xx}(q)/\sigma_{zz}(q)$ for all of those modes approaches ν_2 . To see that the ratio must equal c^2 , note that on large length scales the response appears as two narrow lines that propagate along the directions $x = \pm cz$. Newton's laws require that the stress along these lines correspond to forces directed along the line, which immediately implies $\sigma_{xx} = c^2\sigma_{zz}$ along the line.

The crossover from a roughly standard elastic form to a hyperbolic one with diffusive broadening is an unusual feature. We note that linear elasticity theories, even in the unstable regime where the equations are hyperbolic, always yield scale invariant response functions for a semi-infinite medium. The spectrum is always purely linear, so that the response is a function of x/z only. In the DFCN, however, the spectrum has a richer structure and the response at large z may appear quite different from that at small or modest depths. Though the discrete model studied above does not represent a realistic picture of a disordered granular material, the result does suggest that experimental data should be interpreted cautiously: the appearance of a response with a typical elastic form may be a deceiving effect of working with a relatively small sample.

Fig. 11 shows a contour plot of the response for the second choice of perturbation in Eq. (35). The figure clearly shows the emergence of the double-peaked structure at large z from a single peak at intermediate z . It also shows multiple peaks near $z = 0$ that have not yet been mentioned. These peaks, which are of very low amplitude, form and decay rapidly. The feature in the spectrum that is responsible for them is the broad peak in the uppermost branch of the real part in the neighborhood of $q = 2.5$. (See Fig. 9.) Modes near this value of q decay slightly more slowly than others nearby.

5.2 n -fold symmetric stars in 2D

For sets of star vectors with the symmetry of a regular n -gon, as depicted in Fig. 12, the full nonlinear problem is much more difficult due to the fact that splitting generates chains with different intensities. Nevertheless, analysis of the Boltzmann equation with fusion terms neglected can be carried out and yields useful insights.

When the fusion terms in Eq. (5) are neglected, the equation can be multiplied by f and integrated over f to obtain a new Boltzmann equation governing the spatial variations in the quantity $F(\theta) \equiv \int_0^\infty df f P(f, \theta)$, the *force density* associated with chains in the θ direction. [16] This equation can be analyzed in detail for the case where all chains are directed along the discrete set $\theta_j = 2\pi j/n$ for $0 \leq j < n$, depicted in Fig. 12. Consistency with the

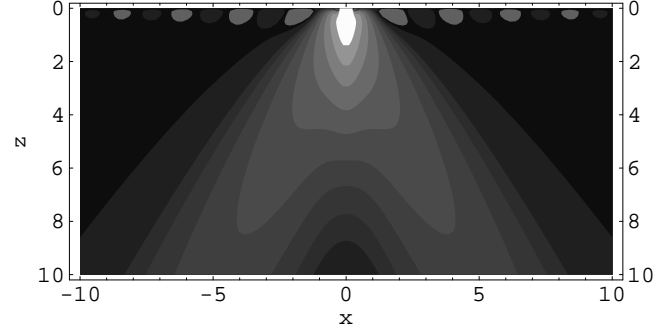


Fig. 11. Contour plot of σ_{zz} for the vertical orientation of 6-fold star vectors at applied chain density $(p_0, p_1, p_5) = (0, 2\epsilon, 2\epsilon) \exp(-(x/0.09)^2)$. The contour lines are at the set of values $(-0.001, 0, 0.001, 0.005, 0.007, 0.01, 0.014, 0.02, 0.028, 0.04, 0.056, 0.08)$. The emergence of the double-peaked structure from a single peak between $z = 0.5$ and 4.0 is clearly visible. For $z < 0.5$, a number of small, rapidly decaying peaks appear corresponding to wavenumbers near the broad peak in the spectrum near $q = 2.5$, which is visible in Fig. 9.

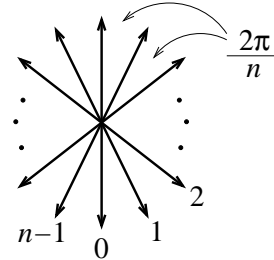


Fig. 12. The n -fold star used for analysis of the linear theory. Each angle is $2\pi/n$, where n is an integer not divisible by 4.

restriction to this discrete set can be maintained by assuming that splittings are always symmetric and outgoing chains make angles of $2\pi/n$ with the incoming one. (For $n > 8$ one can also have splittings at angles of $4\pi/n$, and so on, but the simplest case is sufficient for our purposes.) To avoid the need for special treatment of the horizontal directions, we also consider only n 's that are not multiples of 4.

Let F_j be the force density for chains in the direction $\theta = 2\pi j/n$. After rescaling of λ to unity, the continuum equations for the F 's are

$$\cos(j\theta) \partial_z F_j + \sin(j\theta) \partial_x F_j = -F_j + \frac{1}{2c_1} (F_{j-1} + F_{j+1}), \quad (37)$$

where $\theta \equiv 2\pi/n$, $c_1 \equiv \cos \theta$, and indices are taken modulo n . An analysis of this equation in the slab geometry is presented in the appendix. It shows that the lack of solutions to the linear problem in the 6-fold case is generic: force densities always diverge when the system is sufficiently deep, even though the intensities of the chains become exponentially small after many splittings.

5.3 Three dimensions

In 3D, the analogue of the 120° vertex for splitting and fusing is the tetrahedral vertex. Three types of events are possible: splitting, in which one chain splits into three; fusion, in which three chains fuse into one; and scattering, in which incoming chains along two of the tetrahedral directions produce two outgoing chains along the remaining two directions. In principle, scattering events should be more common than fusions, which require terms in the Boltzmann equation of order P^3 . Scattering events do not change the total force density in the system, however, and therefore are not sufficient to regulate the divergence in the linear theory. Though scattering events should clearly be included in the Boltzmann equation for completeness, fusions are the essential process.

A suitable star of vectors is formed from the 20 vectors pointing to the faces of an icosahedron. (The apparently simpler choice of the star of vectors pointing to the faces of an octahedron turns out to possess certain symmetries that lead to nongeneric behavior.) Each vector on the icosahedral star is a part of two different tetrahedra. One can assume, for example, that the splitting of a chain occurs along each tetrahedral set with probability 1/2.

Choosing the orientation of the icosahedral star to include one vector in the downward vertical direction, and neglecting scatterings, at least one line of fixed points can be found. In this orientation, there is one vector \hat{v} with z -component $s_z = 1$, three with $s_z = \sqrt{5}/3$, six with $s_z = 1/3$, and 10 related to these by inversion. The fixed points can be parametrized by p , with the densities of chains as follows: $P = p^3/\sqrt{2}$ for all $s_z = 1$ chains; $P = p^2/\sqrt{2}$ for all $s_z = \sqrt{5}/3$ chains; $P = p/\sqrt{2}$ for all $s_z = 1/3$ chains; and for all chains related to these by inversion, $P \rightarrow 1/(2P)$. This gives for the “Poisson ratios”

$$\nu_1 = \frac{8r_{1+} + 2r_{2+}}{2r_{1+} + 10r_{2+} + 3r_{3+}}; \quad (38)$$

$$\nu_2 = \frac{8r_{1-} + 4r_{2-}}{2r_{1-} + 20r_{2-} + 9r_{3-}}. \quad (39)$$

ν_1 varies from 2/3 at the fixed point, which is outside the range of stability for a standard, isotropic elasticity theory, to 0 at large p . ν_2 varies from 16/69 to 0 and thus is always within the stable regime.

This preliminary treatment of a 3D model suggests that there is nothing fundamentally different from the 2D models studied above. The spectrum and response functions in the vicinity of a fixed point can be calculated numerically. Extracting the asymptotic form of the response, however, is not as straightforward as in the 2D case. Thorough analyses of the nature of the response and the effects of the scattering terms are beyond the scope of this work.

5.4 Long-wavelength theories for a continuum of chain directions

In Ref. [16], equations for the stress tensor were developed for a directed force chain network without the restriction

to a discrete set of directions. It was shown that for the linear Boltzmann equation, multiplication by f and integration over f could be carried out to obtain equations for the force densities $F(\theta) \equiv \int_0^\infty df fP(f, \theta)$. These in turn could be cast in terms of equations for the stress tensor under the assumption that $F(\theta)$ was nearly isotropic. This assumption is clearly not true on length scales of order λ , but was argued to be true at large length scales. In terms of F , the following three quantities were defined:

$$\begin{aligned} \rho &= \frac{1}{2} \int_{-\pi}^{\pi} d\Omega F(\theta); \\ \mathbf{J} &= \frac{1}{2} \int_{-\pi}^{\pi} d\Omega F(\theta) \hat{\mathbf{n}}; \\ \sigma &= \int_{-\pi}^{\pi} d\Omega F(\theta) \hat{\mathbf{n}} \otimes \hat{\mathbf{n}}, \end{aligned} \quad (40)$$

where $d\Omega = d\theta/2\pi$ as defined above. Here ρ is the hydrostatic pressure, σ is the stress tensor (see Eq. (2), and \mathbf{J} is a vector field that plays a similar mathematical role to the displacement field in standard elasticity theory. Under the assumption that $F(\theta)$ is nearly isotropic, one can express $F(\hat{\mathbf{n}})$ as a linear combination of ρ , $\hat{\mathbf{n}} \cdot \mathbf{J}$, and $\hat{\mathbf{n}} \cdot \sigma \cdot \hat{\mathbf{n}}$, then use Newton’s laws and a compatibility condition on \mathbf{J} to derive a partial differential equation for σ . That equation turned out to be elliptic, which suggested a response similar to that of an elastic material.[16]

From the results of the present work, it appears that the assumption of the isotropy of $F(\theta)$ at large length scales was not justified. Analysis of the linear theory, as discussed in the appendix, shows that the isotropic fixed point $F = 0$ is unstable to perturbations that favor large $F(\theta)$ for θ near $\pi/2$, and that the nontrivial fixed points are generically anisotropic. Thus the analysis presented in Ref. [16] should be generalized to the anisotropic case. It is not clear whether such a generalization can preserve the close correspondence between \mathbf{J} and the displacement field of standard elasticity theory.

In addition to the issue of anisotropy, this program encounters difficulties related to the neglect of the nonlinear terms in the derivation of the equations for $F(\theta)$. Naive attempts to carry out the same program without neglecting the nonlinear terms fail: the structure of the ϕ_f terms in Eq. (5) make it important to calculate the full distribution $P(f, \theta)$. It is not possible, without making further approximations, to recast the equations in terms of $F(\theta)$ alone.[21]

It should also be noted that the implicit passage to the limit of large length scales corresponds to keeping only terms of order q in the expressions for c and D . Such a calculation does not pick up the quadratic dependence of D on q . Thus, in these theories, whenever the response is hyperbolic the apparent value of D is zero, corresponding to delta-functions that propagate without broadening. Inclusion of the terms in the expansion of F containing nonzero wavevectors \mathbf{q} would be required in order to compute D .

6 Discussion

6.1 Numerical simulations

There is no known algorithm for numerically generating configurations that are consistent with the Boltzmann equation. Simulations previously reported [16] were done on small systems and used a regularization scheme that is uncontrolled. The difficulty encountered in these simulations is that the effects of fusions can create “causality” problems: a chain that gives rise to many others through multiple splittings may itself be altered by a fusion with one of its offspring. For small systems, this problem does not occur and the pseudo-elasticity theory derived from the linear Boltzmann equation appears to give a good description response.[16] For large systems, however, it is an important part of the physics. The algorithms used in Ref. [16] for generating DFCN’s grind to a halt when the system size is increased to a few times the length λ , due to the generation of infinite loops associated with fusions.

One approach to avoiding the causality problem would be to neglect fusions altogether. To avoid an exponential explosion in the number of chains (and the total force density), one must then introduce a lower cutoff on force chain intensities. All chains with intensity lower than the cutoff are simply ignored. Again, this approach may be reasonable for small systems where the chains being neglected are just those that were generated in splitting events where one daughter chain was in nearly the same direction as the parent and the other was very weak. For very large systems, however, chains split many times before reaching the bottom. At large depths, the number of chains surviving above the cutoff will eventually decay to zero, so no stress at all will be transmitted to large distances. The apparently justifiable neglect of small forces leads to substantial violations of Newton’s laws.

It appears that the numerical generation DFCN’s will require algorithms for relaxing candidate configurations in a nontrivial way so as to arrive at networks with statistical properties consistent with the Boltzmann equation.

6.2 Strong vs. weak disorder and the importance of discrete directions

Hyperbolic systems with weak disorder yield diffusively broadening, propagating peaks.[4] The strong disorder regime has not previously been accessible. In one respect, our discrete model exhibits strong disorder: splitting events cause chains to rapidly lose memory of the direction of their ancestors. In another sense, though, the disorder may be weak: the orientation of the star vectors exhibits no fluctuations. In any case, the discrete model may apply rather directly to the case of a hexagonal array of disks with a random distribution of vacancies.

We are currently investigating the behavior of the Boltzmann equation for more general splitting and fusing functions. To make predictions for real granular materials that have not been carefully prepared to have orientational order, it is crucial to know whether the hyperbolic response at large depths survives in the absence of a globally specified set of favored directions.

6.3 Boundary conditions

A major unanswered question about the DFCN theory is how to determine the appropriate boundary conditions associated with a particular physical situation. Assume, for example, that we clamp a slab of granular material between two nominally flat pistons. How do we decide whether we are injecting a high density of weak chains or a low density of strong chains? The problem is complicated by the fact that some part of the pressure on the pistons derives from the *response* to the injected chains, so our boundary condition must be chosen so as to produce the correct pressure at the associated fixed point; we cannot simply inject chains corresponding to the desired loading of the surfaces, though in the slab geometry we can always scale all force chain intensities by a common factor to produce any desired total vertical force on the top and bottom boundaries.

6.4 Anisotropy and gravity

As one might expect on symmetry grounds, generic fixed point solutions of the Boltzmann equation in the slab geometry are anisotropic even though the equation does not contain intrinsic symmetry breaking terms, and this anisotropy has a qualitative effect on the response. The source of the differences in response are traceable to the inherent nonlinearity of the system. The response near a given fixed point cannot be construed as the superposition of the response in an isotropic system together with a homogeneous anisotropic deformation.

Inclusion of gravity in the DFCN theory may be accomplished by assuming that every grain is a source of a new vertical chain, which may or may not instantly fuse with other chains passing through the same grain. This would require the addition of a source term to the Boltzmann equation that breaks the isotropy of the equation itself, not just the solutions with anisotropic boundary conditions. Similar considerations would apply for systems with an anisotropic fabric tensor; i.e., systems in which certain directions are favored by an intrinsic anisotropy in the packing geometry. Analysis of systems with intrinsic anisotropy is beyond the scope of this work.

6.5 Standard elasticity

Materials described by standard, linear elasticity theory, even if isotropic, always have Fourier spectra with exponents linear in q . Such theories can produce propagating peaks, as have been observed for ball-and-spring models with strong anisotropy [22]. But the peaks must always broaden linearly, never diffusively. For classically stable materials, the peaks will always broaden linearly with depth. For a semi-infinite slab, there is no parameter in the theory with dimensions of length, so the response is always a function of x/z only. Outside the domain of stability, however, the response may be hyperbolic. We are currently investigating anisotropic models in this regime

in an effort to determine whether they can describe the behavior of DFCN's at very large length scales.[21]

6.6 Interpreting experiments

The emergence of a two-peaked, hyperbolic response at large depths in the models we have studied is quite remarkable, particularly in the vertical orientation of the 6-fold star, where the directions of propagation are not simply related to the star vectors. In a strongly scattering system such as this one, where splittings cause large changes in the directions of force chains, one might naively expect any peaks to be strongly broadened at large depths, which would lead to a single centered peak in the response function. Indeed, this is what we observe for moderate depths: a system may have a two-peaked response close to the surface, but those peaks decay or broaden rapidly, and a single peak emerges. Surprisingly, in the λY -model two peaks that really are associated with hyperbolic response emerge at even greater depths, and the directions of propagation of these peaks are generally not the same as those of the original two peaks near the surface.

Experiments on 2D systems have shown both propagating peaks and single centered peaks.[23,24,25] In interpreting these experiments it is important to note three things: (1) Correlations in the positions of grains at the surface with the layer just below may affect the interpretation of the distribution of chain directions injected at the surface. It would not be surprising to see structure in the response close to the surface, possibly even double peaks due to the immediate splitting of a vertical force chain. (2) For well-ordered systems, the splitting length λ may be large enough so that the entire system is in the very shallow regime. Thus the two peaks observed are not necessarily indicative of a hyperbolic response at large scales. (3) Even for disordered systems, one may have to probe systems an order of magnitude or more larger than λ before the true large system behavior becomes apparent. This may be especially difficult because the peaks decrease in amplitude at large depths, but the fact that diffusively broadening peaks become cleanly separated at large depths offers some hope that they could be resolved in future experiments.

Acknowledgements

We thank J.-P. Bouchaud and M. Otto for extensive discussions and editorial comments, and R. Behringer, E. Clément, E. Kolb, D. Levine, G. Ovarlez, and G. Reydellet for helpful conversations. J.E.S.S. is grateful for the hospitality of the LMDH at Jussieu in Paris, where much of this work was carried out. This work was supported by the grant PICS-CNRS 563, NSF Grants DMS-98-03305 and PHY-98-70028.

References

- R. M. Nedderman, *Statics and kinematics of granular materials* (Cambridge University Press, 1992).
- F. Cantelaube and J. D. Goddard, Elastoplastic arching in granular heaps, in *Powder and Grains 97*, edited by R. P. Behringer and J. T. Jenkins, Rotterdam, 1997, Balkema.
- S. Edwards and D. Grinev, *Physica A* **294**, 57 (2001).
- J.-P. Bouchaud, M. Cates, and P. Claudin, *Journal de Physique I* **5**, 639 (1995).
- P. Claudin, J.-P. Bouchaud, M. Cates, and J. Wittmer, *Physical Review E* **57**, 4441 (1998).
- A. Tkachenko and T. Witten, *Physical Review E* **60**, 687 (1999).
- R. Ball and R. Blumenfeld, *Physical Review Letters*, to appear (2002), cond-mat/0008127.
- G. Combe and J.-N. Roux, *Physical Review Letters* **85**, 3628 (2000).
- D. Head, A. Tkachenko, and T. Witten, *European Physical Journal E* **6**, 99 (2001).
- S. N. Coppersmith, C.-H. Liu, S. Majumdar, O. Narayan, and T. A. Witten, *Physical Review E* **53**, 4673 (1996).
- J. Socolar, *Physical Review E* **60**, 1999 (1999).
- C. Eloy and E. Clément, *Journal de Physique I* **7**, 1541 (1997).
- D. Howell and R. P. Behringer, Fluctuations and dynamics for a two-dimensional sheared granular material, in *Powder and Grains 97*, edited by R. P. Behringer and J. T. Jenkins, Rotterdam, 1997, Balkema.
- F. Radjai, M. Jean, J.-J. Moreau, and S. Roux, *Physical Review Letters* **77**, 274 (1996).
- M. Cates, J. Wittmer, J.-P. Bouchaud, and P. Claudin, *Physical Review Letters* **81**, 1841 (1998).
- J.-P. Bouchaud, P. Claudin, D. Levine, and M. Otto, *European Physical Journal E* **4**, 451 (2001).
- L. D. Landau and E. M. Lifshitz, *Theory of Elasticity*, Third ed. (Pergamon, Oxford, 1986).
- L. Limat, *Physical Review B* **40**, 9253 (1989).
- L. Breton and E. Clément and P. Claudin and J.-D. Zucker, in preparation.
- D. Serero, G. Reydellet, P. Claudin, E. Clément, and D. Levine, *European Physical Journal E* **6**, 169 (2001).
- M. Otto, P. Claudin, J.-P. Bouchaud, and J.E.S. Socolar, in preparation.
- C. Goldenberg and I. Goldhirsch, cond-mat/0108297 (2001).
- J. Geng *et al.*, *Physical Review Letters* **87**, 035506 (2001).
- G. Reydellet and E. Clément, *Physical Review Letters* **86**, 3308 (2001).
- D. Blair, N. Mueggenburg, A. Marshall, H. Jaeger, and S. Nagel, *Physical Review E* **63**, 041304 (2001).

A Failure of the linear theory near the origin

In this appendix we present an analysis of the linear Boltzmann equation for a discrete set of chain directions and symmetric splittings. The main purpose is to clarify the nature of the divergence and hence the failure of the linear theory.

A.1 The equations and their solutions

Let F_j be the density of force chains with direction $\theta = 2\pi j/n$, where n is an integer that is not a multiple of 4

and $\theta = 0$ corresponds to the positive z direction. (See Fig. 12.) Assume that splittings always occur at an angle $\theta = 2\pi/n$; i.e., when a chain in the j direction splits, the only option is to produce chains in the $j-1$ and $j+1$ directions. Eq. (37), reproduced here, governs the force densities.

$$\cos(j\theta) \partial_z F_j + \sin(j\theta) \partial_x F_j = -F_j + \frac{1}{2c_1} (F_{j-1} + F_{j+1}). \quad (41)$$

We seek solutions to this equation in the slab geometry with a load that is uniform in the horizontal direction.

Translational invariance ensures that the solution will be uniform in the horizontal direction, so the ∂_x terms vanish. Letting c_j stand for $\cos(j\theta)$, we have

$$\partial_z F_j = -\frac{1}{c_j} F_j + \frac{1}{2c_1 c_j} (F_{j-1} + F_{j+1}). \quad (42)$$

In matrix form,

$$\partial_z \mathbf{F} = \mathbf{M} \cdot \mathbf{F}, \quad (43)$$

where \mathbf{F} is the n -dimensional vector with elements F_j and

$$\mathbf{M} = \begin{pmatrix} \frac{1}{c_0} & \frac{1}{2c_1 c_0} & 0 & \cdots & 0 & \frac{1}{2c_1 c_0} \\ \frac{1}{2c_1 c_1} & \frac{1}{c_1} & \frac{1}{2c_1 c_1} & 0 & \cdots & \\ 0 & \frac{1}{2c_1 c_2} & \frac{1}{c_2} & \frac{1}{2c_1 c_2} & 0 & \cdots \\ \vdots & & \ddots & \ddots & \ddots & \\ \frac{1}{2c_1 c_{n-1}} & 0 & \cdots & 0 & \frac{1}{2c_1 c_{n-1}} & \frac{1}{c_{n-1}} \end{pmatrix}. \quad (44)$$

\mathbf{M} is tridiagonal (except for the entries in the corners), but *not* symmetric. Its eigenvectors are not orthogonal, nor do they span the full space. One can check that both

$$\mathbf{C}^{(2)} \cdot \mathbf{M} = 0 \quad (45)$$

and

$$\mathbf{X}^{(2)} \cdot \mathbf{M} = 0, \quad (46)$$

where $\mathbf{C}^{(2)}$ and $\mathbf{X}^{(2)}$ are the (row) vectors with components c_j^2 and $c_j \sin(j\theta)$, respectively. This implies that $\mathbf{C}^{(2)}$ and $\mathbf{X}^{(2)}$ are orthogonal to every eigenvector of \mathbf{M} with a nonzero eigenvalue, and therefore that no matter how those eigenvectors grow or shrink with increasing z , the projection of their sum onto $\mathbf{C}^{(2)}$ and $\mathbf{X}^{(2)}$ will be constant determined by the amplitudes of the eigenvectors with eigenvalue zero. These projections corresponds to σ_{zz} and σ_{xz} , and their invariance is a direct consequence of Newton's laws.

The matrix \mathbf{M} can be block diagonalized to separate subspaces that are symmetric or antisymmetric with respect under $j \rightarrow n-j$. For present purposes, it is sufficient to consider only the symmetric subspace. Let \mathbf{M}_s denote the $m \times m$ matrix corresponding to the symmetric block. For n odd, we have $m = (n+1)/2$ and for n even $m = (n/2) + 1$. \mathbf{M}_s has two eigenvalues equal to zero. One is associated with the eigenvector \mathbf{C} with elements $F_j = c_j$. The other is associated with a vector \mathbf{E}_1 that satisfies $\mathbf{M} \cdot \mathbf{E}_1 = \mathbf{C}$ rather than the usual eigenvalue equation $\mathbf{M} \cdot \mathbf{E} = \lambda \mathbf{E}$. One can check that the solution

is $\mathbf{E}_1 = b(1, 1, 1, \dots) - a\mathbf{C}^{(2)}$, with $a = c_1/(c_1 - c_2)$ and $b = a(1 - c_1)$.

The solution of the differential equations for an arbitrary initial condition within the symmetric subspace is

$$\mathbf{F} = a_0 \mathbf{C} + a_1 (\mathbf{E}_1 + z\mathbf{C}) + \sum_{k=2}^{m-1} a_k e^{\lambda_k z} \mathbf{E}_k, \quad (47)$$

where the a_k 's are determined by the boundary conditions. We emphasize the following three features of the solutions. First, projections onto \mathbf{C} are *not* conserved as z varies, even though the eigenvalue associated with \mathbf{C} is zero, because \mathbf{C} appears also multiplied by z . Second, symmetry under $z \rightarrow -z$ and $F_j \rightarrow F_{n/2-j}$ guarantees that if λ is an eigenvalue of \mathbf{M}_s , $-\lambda$ is also, implying that, aside from the eigenvectors with zero eigenvalues, half of the eigenvectors grow exponentially with increasing z . Finally, all the \mathbf{E}_k 's except \mathbf{E}_1 must have both positive and negative components, since their projection onto the positive definite $\mathbf{C}^{(2)}$ vanishes.

A.2 Negative force densities and their origin

To avoid negative force densities in a deep system, the boundary values of \mathbf{F} must have zero projection on all eigenvectors with positive eigenvalues. Since $\sigma_{zz} = \mathbf{C}^{(2)} \cdot \mathbf{F}$, any boundary condition at $z = 0$ that has nonvanishing σ_{zz} must have $a_1 \neq 0$. But this implies that the $z\mathbf{C}$ term in Eq. (47) cannot be avoided. Since \mathbf{C} has negative components, and all the contributions from eigenvectors with negative eigenvalues decrease with increasing z , the solution will always produce negative force densities at sufficiently large z .

The appearance of negative force densities may be counter-intuitive. After all, the linear equations describe physically allowable processes that can never generate negative densities of chains and never yield negative intensities for any chain. The source of the negative F 's in the solution is a divergence that occurs when the system is sufficiently deep to allow enough splittings that an appreciable fraction of the descendants of a downward-pointing chain are directed upwards. This causes an exponential explosion in the number of chains in the system and a consequent divergence of the force densities. Even though the intensities of the descendants of a given chain decrease exponentially with generation number, the sum of their intensities diverges because in every splitting event from a chain with intensity f_1 to two with f_2 and f_3 we have $(f_2 + f_3)/f_1 = \sec(\theta) > 1$. The effect on the solutions to the differential equations is roughly analogous to the continuation of $\sum_{m=0}^{\infty} r^m = 1/(1-r)$ beyond its radius of convergence $r = 1$, where it appears that an infinite sum of positive terms gives a negative result. In other words, the theory is not well defined for slabs of thickness larger than a “persistence length” for chain directions.

A.3 The question of anisotropy at large scales

The problem of negative densities in the linear theory shows that the response of the DFCN system can only be properly defined for a pre-stressed system. This still leaves open the possibility that the same linear theory might describe deviations from some uniformly stressed state.

Here we point out that in the slab geometry with uniform horizontal loading, the instability of the trivial solution, $F = 0$, to the linear equations leads to anisotropic F 's for a broad class of splitting functions ψ_s . For discrete n -fold systems in which symmetric splittings ($\theta_2 = \theta_3$) are allowed with uniform probability for all angles up to $\theta_2 = \pi/3$, numerical diagonalization of the matrix \mathbf{M} of Eq. (44) shows that the most strongly unstable $q = 0$ modes correspond to eigenvectors $E(\theta)$ peaked near $\theta = \pm\pi/2$. The eigenvalues grow more unstable and the eigenvectors more sharply peaked as n increases toward the continuum limit. Analytical arguments have also been obtained for certain special choices of $\psi_s(\theta_2, \theta_3)$.

The anisotropic nature of this instability casts doubt on the validity of the conjecture that the DFCN should appear isotropic on large scales. The isotropic DFCN does not appear to be an attractor for any but a perfectly tuned set of initial conditions.